Numerical simulation of a viscoelastic fluid with anisotropic heat conduction

NUMERICAL SIMULATION OF A VISCOELASTIC FLUID WITH ANISOTROPIC HEAT CONDUCTION

P. WAPPEROM and M.A. HULSEN
Delft University of Technology, Laboratory for Aero and Hydrodynamics, Rotterdamseweg 145, 2628AL Delft, The Netherlands

Abstract. For the nonisothermal flow of a viscoelastic fluid we have taken into account temperature dependency of the relaxation times and the viscosities in the constitutive equation for the stress. In the energy equation the heat flux is specified by Fourier's law, where anisotropic heat conduction has been taken into account. Furthermore one has to specify which part of the stress work is dissipated and which part is stored as elastic energy. The equations are solved with a finite element method for the balance equations and a streamline integration method for the constitutive equation. The influence of the Deborah number, the Péclet number and the cooling temperature are examined in a flow through a 4 to 1 contraction.

Key words: shift factors, dissipation, anisotropic heat conduction, finite elements, streamline integration, axisymmetrical 4 to 1 contraction

1. Introduction

In the last 15 years much attention has been paid to the numerical simulation of isothermal flows of viscoelastic fluids. For recent reviews see Crochet (1989) and Keunings (1989). For steady problems the use of streamline integration methods made it possible to solve the equations for high Deborah numbers. Relatively small numbers of publications have appeared in on nonisothermal flows of viscoelastic fluids, especially not for high Deborah numbers. Therefore we extended the streamline integration method of Hulsen & van der Zanden (1991) to nonisothermal flows.

In section 2 of this article the general differential equations describing a nonisothermal viscoelastic flow are given. It starts with a short overview of the conservation laws we have used. Then we describe the constitutive equations for the stress and heat flux. For the stress equation we take into account that the viscosity and relaxation time depend on the temperature. The heat flux will be described with Fourier's law, where the heat conduction may be anisotropic. In the derivation of a temperature equation from the conservation of energy one has to specify which part of the stress work is dissipated and which part is stored as elastic energy. Section 3 describes the numerical implementation of the equations for nonisothermal, viscoelastic fluid flows. The finite element method (FEM) has been used to solve the momentum and temperature equations and a streamline integration method to solve the constitutive equation for the stress. Section 4 describes the boundary conditions of the 4 to 1 contraction and the characteristic quantities. The results of our calculations can be found in section 5. Finally some conclusions are given in section 6.

2. Basic Equations

2.1. Conservation Laws

In this subsection we give a short description of the four balance equations we have used to describe the nonisothermal flow of a fluid. We will assume that the density of the fluid ρ is constant and that the flow is steady. Furthermore we will neglect body forces in the momentum equations and external heat sources in the energy equation. This leads to the following equations in a fixed bounded space Ω

- conservation of mass
$$\nabla \cdot \underline{v} = 0, \tag{1}$$
- balance of momentum
$$\rho \underline{v} \cdot \nabla \underline{v} + \nabla p = \nabla \cdot \underline{\underline{\tau}}, \tag{2}$$
in which $\underline{v}$ is the velocity, ρ the density, p the pressure and $\underline{\underline{\tau}}$ the extra-stress tensor. Note that the total stress $\underline{\underline{\sigma}}$ has been split into an isotropic part $p\underline{\underline{I}}$ and a deviatoric part $\underline{\underline{\tau}}$.
- balance of moment of momentum
$$\underline{\underline{\tau}} = \underline{\underline{\tau}}^T \tag{3}$$
- balance of energy
$$\rho \underline{v} \cdot \nabla u = \underline{\underline{\tau}} : \underline{\underline{d}} - \nabla \cdot \underline{\phi}_q, \tag{4}$$
where u is the internal energy and $\underline{\phi}_q$ the heat flux vector.

In these equations there are two quantities that must be specified by a constitutive equation, the stress and the heat flux. Furthermore we need an expression for the temperature instead of the energy, because some parameters depend on the temperature. These will be the topics of the section 2.2.

2.2. Constitutive Equations

2.2.1. Stress

The extra-stress tensor $\underline{\underline{\tau}}$ is determined by the deformation history of a fluid particle and has to be specified by a constitutive equation. For viscoelastic fluids it consists of a contribution of the Newtonian solvent and a contribution of the polymer part. To fit the behaviour of the polymeric part well, it is often necessary to consider multi-mode models:

$$\underline{\underline{\tau}} = 2\eta_s \underline{\underline{d}} + \sum_{k=1}^{K} \underline{\underline{\tau}}_k, \tag{5}$$

in which η_s is the solvent viscosity, K the number of modes and Euler's rate of deformation tensor $\underline{\underline{d}} = (\underline{\underline{L}} + \underline{\underline{L}}^T)/2$, with the velocity gradient $\underline{\underline{L}}^T = \nabla \underline{v}$. A substress $\underline{\underline{\tau}}_k$ can be specified by a differential or integral equation. In this article we will use a differential model, the Giesekus model. The differential equation will be given in terms of an internal deformation tensor $\underline{\underline{b}}_k$, as used in the derivation of the Giesekus model by Giesekus (1982). This is a more convenient form to derive an expression for the dissipation as described in section 2.2.3. Furthermore it will be used in the expression for the heat flux vector in section 2.2.2. It can be proved that $\underline{\underline{b}}_k$ is a

positive definite tensor, see Hulsen (1990). For the Giesekus model the stress tensor $\underline{\underline{\tau}}_k$ can then be found from the internal deformation tensor $\underline{\underline{b}}_k$ by

$$\underline{\underline{\tau}}_k = \frac{\eta_k}{\lambda_k} \left(\underline{\underline{b}}_k - \underline{\underline{I}} \right), \tag{6}$$

where λ_k is the relaxation time and η_k the viscosity of mode k. In terms of the internal deformation tensor, the Giesekus model reads

$$\lambda_k \overset{\triangledown}{\underline{\underline{b}}}_k + \left(\underline{\underline{I}} + \alpha_k \left(\underline{\underline{b}}_k - \underline{\underline{I}} \right) \right) \cdot \left(\underline{\underline{b}}_k - \underline{\underline{I}} \right) = \underline{\underline{0}}, \tag{7}$$

with the upper convected derivative defined as

$$\overset{\triangledown}{(\,)} = \dot{(\,)} - \underline{\underline{L}} \cdot (\,) - (\,) \cdot \underline{\underline{L}}^T. \tag{8}$$

The constants $0 \leq \alpha_k < 1$ denote the amount of anisotropic drag. For $\alpha_k = 0$ the drag is isotropic and the model then reduces to the multi-mode upper-convected Maxwell model. The amount of anisotropy increases with increasing α_k.

The only parameters that are assumed temperature dependent are the viscosities and relaxation times. This temperature dependency is given by a shift factor a_T with which these parameters are multiplied. In our examples in section 5 there is no Newtonian viscosity. In principle the shift of the multi-mode viscosities and relaxation times can be chosen different for each mode:

$$\left.\begin{aligned} \log\left(\tfrac{\eta_k}{\eta_{k,\mathrm{ref}}}\right) &= \log a_{T,k}, \\ \log\left(\tfrac{\lambda_k}{\lambda_{k,\mathrm{ref}}}\right) &= \log a_{T,k}, \end{aligned}\right\} \quad k = 1, \ldots, K, \tag{9}$$

where the subscript $_{\mathrm{ref}}$ denotes a parameter at reference temperature. In section 5, however, we will use the same Andrade shift factor for each mode:

$$\log a_T = c_1 \left(\frac{1}{T} - \frac{1}{T_{\mathrm{ref}}} \right), \tag{10}$$

where c_1 is a shifting constant and T_{ref} the reference temperature.

2.2.2. Heat Flux

The heat flux vector in equation (4) has to be specified by a constitutive equation. A widely used constitutive equation is Fourier's law, which has the general form

$$\underline{\phi}_q = -\underline{\underline{\kappa}} \cdot \nabla T, \tag{11}$$

where the heat conduction tensor $\underline{\underline{\kappa}}$ can be a function of temperature and the internal deformation tensor. In this article we assume that it only depends on the internal deformation tensor. Mostly an isotropic heat conduction is assumed. Measurements of the heat conductivity by Hands (1982) and Washo & Hansen (1969), however, show that the increase in the direction of the orientation, and a corresponding decrease in the directions perpendicular to it, can be considerable.

For a one mode model the most general model that can be obtained for the heat conduction tensor, is

$$\underline{\underline{\kappa}} = \kappa_0 \underline{\underline{I}} + \kappa_1 \underline{\underline{b}} + \kappa_2 \underline{\underline{b}}^{-1}, \tag{12}$$

where the scalars κ_0, κ_1 and κ_2 are only functions of the temperature and the invariants I_1, I_2 and I_3 of the internal Finger tensor $\underline{\underline{b}}$. In equilibrium state the internal Finger tensor equals $\underline{\underline{b}} = \underline{\underline{I}}$ and the heat conduction tensor reduces to

$$\begin{aligned} \underline{\underline{\kappa}} &= \kappa_{\rm eq} \underline{\underline{I}}, \\ \kappa_{\rm eq} &= \kappa_0 + \kappa_1 + \kappa_2, \end{aligned} \tag{13}$$

where $\kappa_{\rm eq}$ is the heat conduction coefficient that would be measured in the equilibrium state. If $\kappa_2 = 0$ is taken in (12) the heat conduction tensor reduces to the model for the expression for a Maxwell fluid, derived from microrheological considerations by van den Brule (1989, 1990).

If no interaction between different modes is assumed the heat conduction tensor for multi-mode models may be written as

$$\underline{\underline{\kappa}} = \kappa_0 \underline{\underline{I}} + \sum_{k=1}^{K} \left(\kappa_{1,k} \underline{\underline{b}}_k + \kappa_{2,k} \underline{\underline{b}}_k^{-1} \right), \tag{14}$$

where K is the number of modes. In principle $2K + 1$ coefficients for the heat conduction tensor have to be determined as a function of temperature and the invariants of $\underline{\underline{b}}_k$. In equilibrium state the heat conduction tensor reduces to

$$\begin{aligned} \underline{\underline{\kappa}} &= \kappa_{\rm eq} \underline{\underline{I}}, \\ \kappa_{\rm eq} &= \kappa_0 + \sum_{k=1}^{K} \kappa_{1,k} + \kappa_{2,k}. \end{aligned} \tag{15}$$

From the restriction that the production of entropy Π_s must be positive for all possible processes, it follows that the contribution of the heat flux must be positive:

$$T \Pi_s = T^{-1} \underline{\underline{\kappa}} : \nabla T \nabla T + \text{o.t.} \geq 0. \tag{16}$$

For a derivation see for example Leonov (1987). To fulfil the inequality it is sufficient to require

$$\left.\begin{array}{rcl} \kappa_0 & \geq & 0, \\ \kappa_{1,k} & \geq & 0, \\ \kappa_{2,k} & \geq & 0, \end{array}\right\} \qquad k = 1, \ldots, K.$$

In the derivation use has been made of the positiveness of the tensor $\underline{\underline{b}}_k$ and the assumption that there is no mutual interaction between the $\underline{\underline{b}}_k$.

2.2.3. Dissipation

Calculation of a temperature equation from the energy equation is straightforward for a Newtonian fluid. Substitution of $u = c_p T$ in the energy equation then gives an equation for the temperature:

$$\rho c_p \underline{v} \cdot \nabla T = D_m - \nabla \cdot \underline{\phi}_q, \tag{17}$$

where the mechanical dissipation D_m equals the total amount of work: $\underline{\underline{\tau}} : \underline{\underline{d}}$. Viscoelastic fluids however, are able to store elastic energy. These elastic energy contributions do not contribute to the mechanical dissipation.

To determine the dissipative and the elastic part of the energy, we use the matrix formulation used by Jongschaap (1991). Under isothermal conditions Jongschaap assumes that the mechanical dissipation is equal to the stress work minus the change of the free energy f per unit mass:

$$D_m = \underline{\underline{\tau}} : \underline{\underline{d}} - \rho \sum_{k=1}^{K} \frac{\partial f}{\partial \underline{\underline{b}}_k} : \dot{\underline{\underline{b}}}_k. \tag{18}$$

Note that for fully developed flows this definition for the dissipation results in a dissipation which is equal to the stress work.

Jongschaap introduces a way to calculate the free energy, which results in a positive dissipation. It is based on a macroscopic time reversal: a change of sign of $\underline{\underline{d}}$. Then all variables are split in an odd and an even part with respect to this macroscopic time reversal. Since the dissipation has to be positive, it is even with respect to this time reversal. Furthermore the velocity gradient is odd and the change in free energy is even, because it does not depend directly on $\underline{\underline{L}}$. Then we can calculate the odd part of the stress and the even part of the rate of change of the internal deformation tensor, which determine the free energy and the dissipation.

Performing the calculation for the Giesekus model (7) gives the following expression for the dissipation and the free energy

$$\begin{aligned} D_m &= 2\eta_s \underline{\underline{d}} : \underline{\underline{d}} + \sum_{k=1}^{K} \frac{\eta_k}{2\lambda_k^2} \left((1-\alpha_k) \left(I_{1,k} + \operatorname{tr} \underline{\underline{b}}_k^{-1} - 6 \right) + \alpha_k \left(\underline{\underline{b}}_k : \underline{\underline{b}}_k - 2I_{1,k} + 3 \right) \right), \\ \rho f &= \sum_{k=1}^{K} \frac{\eta_k}{\lambda_k} \left(I_{1,k} - \ln I_{3,k} \right). \end{aligned} \tag{19}$$

3. Numerical implementation

In this section we describe the numerical methods we have used to solve the equations described in section 2. The system of equations has been decoupled into 3 parts, which are solved iteratively. Each iteration consists of three steps. In the first step we perform an iteration for the equations of motion. In the second step we perform an iteration for the temperature equation. In the last step we perform an iteration for the stress equation. The details of these three steps of the iteration scheme can be found in subsections 3.1, 3.2 and 3.3. The equations of motion and the temperature equation form the elliptic part of the problem. They have been solved with a standard finite element method. The stress constitutive equation is a hyperbolic equation. It has been solved with a streamline integration method. In the following subsections we give for each equation a short description of its numerical implementation and some problems that arise.

3.1. Equations of Motion

To solve the equations of motion we have used an extended quadratic element: the well known Crouzeix-Raviart element. See figure 1. The velocities in the centre point and the pressure derivatives can be eliminated on element level. To eliminate the pressure p in the centre point the penalty method has been used. Instead of the divergence equation (1)

$$\epsilon_p p + \nabla \cdot \underline{v} = 0, \tag{20}$$

is used. The penalty parameter ϵ_p is a small parameter, such that $\epsilon_p p$ is of the order 10^{-6} to 10^{-8}.

To solve the discretized equations of motion, we use an incremental formulation for the resulting matrix-vector equation:

$$\left(\eta_{\rm it} S_v + M_v(U^i) + C_v\right) \Delta U^{i+1} = -R_v(U^i, \Upsilon^i, T^i), \tag{21}$$

where the Picard iteration matrix contains contributions of a proper linearisation of the convective terms M_v, the penalty matrix C_v and a viscous matrix $\eta_{\rm it} S_v$. The iteration viscosity $\eta_{\rm it}$ only slows down the iteration process. For our calculations in section 5 we used $\eta_{\rm it} = 2\eta_0$, where η_0 is the zero-shear-rate viscosity at the lowest temperature in the flow. The increment of the velocities ΔU^{i+1} is defined by

$$\Delta U^{i+1} = U^{i+1} - U^i. \tag{22}$$

The residual $R_v(U^i, \Upsilon^i, T^i)$ depends on the discrete velocities U^i, temperatures T^i and stresses Υ^i of a former iteration step:

$$\begin{aligned} R_v(U^i, \Upsilon^i, T^i) \;=\; & \left(\eta_s(T^i) + \eta_{\rm co}\right) S_v U^i + N_v(U^i) + \\ & C_v U^i - F_v + Q(\Upsilon^i - 2\eta_{\rm co}\bar{D}^i). \end{aligned} \tag{23}$$

N_v contains the contribution of the convective terms, F_v the contributions of the boundary integrals due to the natural boundary conditions and Q the contributions of the divergence of the substresses. From this last term we have to subtract an extra diffusive term based on the nodal point averages of the velocity gradient $\bar{D}^i$. An analogous term based on the non-averaged velocity gradients is added to the contribution of the solvent. This extra viscosity is necessary to avoid almost zero effective viscosities, which may arise due to the use of averaged velocity gradients for streamline integration. Introduction of $\eta_{\rm co}$ improves the condition of the system but increases the viscosity of 'short wavelength' velocity modes.

For checking convergence two conditions have to be satisfied. The first condition is related to the increment of the velocity and the second to the residual of the momentum equation:

$$\begin{aligned} \frac{\max_j |\Delta U_j^{i+1}|}{\max_j |U_j^{i+1}|} &\leq \epsilon_{v,\rm inc}, \\ \frac{||R_v(U^i, T^i)||_f}{||R_v(U^i, T^i)||_t} &\leq \epsilon_{v,\rm res}, \end{aligned} \tag{24}$$

where the maximum norm has been taken over all nodal points j. The norm $||\cdot||_f$ denotes the Euclidean norm over the free degrees of freedom, without the essential

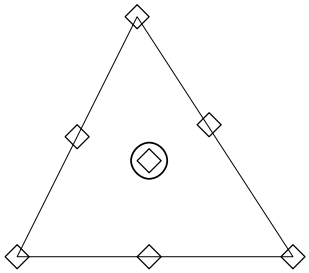

Fig. 1. Crouzeix-Raviart element with seven velocity points (diamonds) and one point with the pressure and its derivatives (circle).

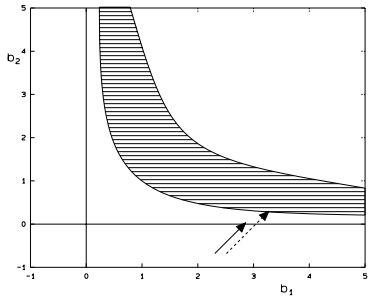

Fig. 2. Correction of the internal deformation tensor in 2D. b_1 and b_2 are the principal values of $\underline{\underline{b}}$. The solution of the model lies in the dashed area, which is bounded by two lines with constant I_3. The straight arrow is the projection on the first quadrant used by Hulsen & van der Zanden (1991). The dashed arrow is a projection on the lowest possible I_3, which is necessary to calculate the dissipation.

boundary conditions. The norm $||\cdot||_t$ denotes the Euclidean norm over the total degrees of freedom, including the essential boundary conditions. For our calculations in section 5 we have taken $\epsilon_{v,\mathrm{inc}} = \epsilon_{v,\mathrm{res}} = 10^{-3}$.

3.2. Stress Equations

The Giesekus model can be written as a set of ordinary differential equations for the internal deformation tensor, by applying the method of characteristics

$$\frac{d\underline{\underline{b}}_k}{ds}\frac{ds}{dt} = -\frac{1}{\lambda_k(T)}\left(\underline{\underline{L}}\cdot\underline{\underline{b}}_k + \underline{\underline{b}}_k\cdot\underline{\underline{L}}^T + \underline{\underline{I}} + \alpha_k\left(\underline{\underline{b}}_k - \underline{\underline{I}}\right)\cdot\left(\underline{\underline{b}}_k - \underline{\underline{I}}\right)\right), \tag{25}$$

where s is a streamline parameter. Integration is performed with a fourth order Runge-Kutta scheme. Below we summarize some important aspects of the streamline integration method and the difficulties that may arise. More details about the isothermal streamline integration can be found in Hulsen & van der Zanden (1991).

- *Computation of the streamlines.*
  From the quadratic velocities of the FEM-part we calculate a quadratic stream function. With this stream function we calculate a piecewise quadratic streamline.
- *Initial conditions.*
  For the integration of (25) we have to specify an initial condition for the internal deformation tensor. There are 3 possibilities. Firstly the streamline may cross an inflow boundary. Secondly the streamline may cross an element where it has already been computed. Finally, to reduce the computing time, the integration is stopped if the travel time is longer than $3\lambda_k(T)$, the relaxation time at the starting point. The initial values are then found by interpolation from the nodal point values of the previous iteration.

- *Stepsize limitations.*
  The limitation of the stepsize of streamline integration is based on the linearized form of equation (7). Furthermore it is possible to limit the stepsize further when the change of a quantity during a step is too large. For example it is necessary to limit the change in velocity gradient at start-up for high values of the Deborah number.
- *Shear flow correction.*
  On the wall numerical approximation errors may cause large false elongational stresses for high Deborah numbers. This can be avoided by imposing an exact simple shear flow on the wall.
- *Correction of the internal deformation tensors.*
  Due to numerical approximation errors the internal deformation tensor can become indefinite in regions where large gradients are present, for example near sharp corners. Due to the Lange residence time near the wall, negative determinants may blow up the quadratic term in (7). To avoid these nonlinear instabilities we correct the internal deformation tensor with an isotropic term. See figure 2. For the stress equation it is sufficient to put $\underline{\underline{b}}$ back on one of the axes, so it becomes semi-positive definite. However for the calculation of the dissipation this is not sufficient, because we need the inverse of the $\underline{\underline{b}}$ tensor in equation (19). For some other models it is possible to find a sharper lower bound for the determinant of $\underline{\underline{b}}$. For the Leonov model, for example, the determinant always equals $I_3 = 1$ and for the Phan-Thien/Tanner model $I_3 \geq 1$. This can be used to make a projection on the curve $I_3 = 1$ instead of one of the principal axes. For the 2D Giesekus model it is also possible to find a lower bound which depends on the parameter α in the Giesekus model (see Hulsen (1988)). However for the 3D axisymmetrical Giesekus model we were not able to find such a lower bound and had to proceed differently. If the determinant of the internal deformation tensor is smaller than 10^{-6} we took the stress work of the specific mode instead of the dissipation. In our examples in section 5 we had to take the stress work for points near the sharp corner of the first two modes, the ones with the largest elasticity.

3.3. Temperature Equation

To solve the temperature equation we have used a quadratic element. For the interpolation of quantities to the Gauss integration points we use quadratic interpolation. The quadratic interpolation may destroy the positive definiteness of the internal deformation tensor. This can give rise to large numerical errors in terms where the inverse of $\underline{\underline{b}}$ has to be calculated. Therefore all quantities that depend on $\underline{\underline{b}}^{-1}$ must first be calculated in the nodal points and can only then be interpolated to the integration points.

For convection dominated problems the standard Galerkin method can give rise to unphysical solutions, with a globally oscillating character. For our type of problems the temperature equation is often convection dominated due to the small value of the diffusivity of a viscoelastic material. The value for our examples in section 5 is $\frac{\kappa}{\rho c_p} = \mathcal{O}(10^{-7})$. To avoid the unphysical wiggles the value of the mesh Péclet number must fulfil in all elements the severe condition $Pe_m = \frac{\rho c_p v \Delta x}{\kappa_v} \leq 2$, where v,

Δx and κ_v are the velocity, the size of the element and the heat conduction in the streamwise direction. To fulfil this restriction the size of the elements of the mesh must be extremely small. This limits of course the practical use of the Galerkin method. To avoid extreme mesh refinement for high values of the mesh Péclet number an upwind technique can be used. The wiggles can be suppressed with help of such methods, but they can cause inaccurate solutions through the introduction of false (extra) diffusion, especially for coarse grids. The false diffusion reduces when the element size becomes smaller.

For the consistent upwind methods all terms are multiplied with an upwind test function ψ_u and added to the weak formulation of the temperature equation.

$$\int_\Omega \left(\rho c_p \underline{v} \cdot \nabla T - D_m - \nabla \cdot (\underline{\underline{\kappa}} \cdot \nabla T)\right)(\psi + \psi_u)\, d\Omega = 0, \qquad \forall \psi \in \Psi^t, \quad \forall \psi_u \in \Psi_u^t. \tag{26}$$

These upwind testfunctions consist of an upwind direction that determines the direction of the upwinding and an upwind function that determines the amount of upwinding.

The Streamline upwind Petrov-Galerkin method (SUPG) has been described by Hughes & Brooks (1982). They take the streamlines as the upwind direction,

$$\psi_u = \tau \underline{v} \cdot \nabla \psi, \tag{27}$$

so this upwind method shows no false crosswind diffusion. With this choice of ψ_u sufficiently smooth exact solutions can be approximated very well. The presence of sharp layers can create local oscillations, in contrary to the standard Galerkin method which creates globally-propagating oscillations. The local wiggles can be suppressed by adding some diffusion in the direction of the temperature gradient as described by Mizukami & Hughes (1985). However for anisotropic heat conduction this method does not work, because the direction of the heat flux does not equal the direction of the temperature gradient.

The upwind function τ indicates the amount of upwinding. It is based on an element Péclet number β_u

$$\begin{aligned} \beta_u &= \frac{||\underline{v}|| h \rho c_p}{2\kappa_v}, \\ \kappa_v &= \frac{\underline{v} \cdot \underline{\underline{\kappa}} \cdot \underline{v}}{||\underline{v}||^2}, \end{aligned} \tag{28}$$

where h is the maximum distance in the element in the direction of $\underline{v}$ and κ_v is a measure for the heat conduction in the streamwise direction. If $\beta_u < 1$ the upwind function can be chosen small, because the standard Galerkin approach still gives accurate solutions. For $\beta_u > 1$ however, upwinding has to be applied to avoid unphysical wiggles. Several choices for τ are used in the literature. We have used the 'optimal' upwind function for the examples in section 5.

$$\begin{aligned} \tau &= \frac{h \xi_u}{2||\underline{v}||}, \\ \xi_u &= \coth \beta_u - \frac{1}{\beta_u}, \end{aligned} \tag{29}$$

where ξ_u is a non-dimensional numerical diffusivity. The choice of τ seems not of great importance. In our test examples we could not find significant differences between different choices of τ.

To solve the discretized temperature equation we also use an incremental formulation. All of the matrices and vectors may contain contributions of the upwind scheme:

$$\left(\kappa_{\rm it} S_T(\Upsilon^i) + M_T(U^i, T^i)\right) \Delta T^{i+1} = -R_T(U^i, \Upsilon^i, T^i). \tag{30}$$

The Picard iteration matrix contains contributions of the convective terms M_T and a diffusive matrix $\kappa_{\rm it} S_T$. The iteration diffusivity $\kappa_{\rm it}$ slows down the iteration process. This avoids convergence problems. A constant and isotropic iteration diffusivity gives good results for our examples in section 5. The increment ΔT^{i+1} is defined by

$$\Delta T^{i+1} = T^{i+1} - T^i, \tag{31}$$

and the residual $R_T(U^i, \Upsilon^i, T^i)$ equals

$$R_T(U^i, \Upsilon^i, T^i) = S_T(\Upsilon^i) T^i + N_T(U^i, T^i) - F_T(U^i, \Upsilon^i, T^i). \tag{32}$$

where the diffusive matrix $S_T(\Upsilon^i)$ may depend on the stresses due to the anisotropic heat conduction. N_T contains the contributions of the convective terms. The dissipation and the boundary integrals of the natural boundary conditions contribute to F_T.

For checking convergence two conditions analogous to the momentum equations have to be satisfied. The first condition is related to the increment of the temperature and the second to the residual of the temperature equation:

$$\begin{aligned} \frac{\max_j |\Delta T_j^{i+1}|}{\max_j |T_j^{i+1}|} &\leq \epsilon_{T,\rm inc}, \\ \frac{||R_T(U^i, T^i)||_f}{||R_T(U^i, T^i)||_t} &\leq \epsilon_{T,\rm res}, \end{aligned} \tag{33}$$

where the maximum norm has again been taken over all nodal points j. The norms $||\cdot||_f$ and $||\cdot||_t$ again denote the Euclidean norm over the free and total degrees of freedom. For our calculations presented in section 5 we have taken $\epsilon_{T,\rm inc} = \epsilon_{T,\rm res} = 10^{-3}$.

3.4. Boundary conditions

This last part of the numerical implementation deals with the boundary conditions. Especially the boundary conditions at the inflow and outflow:

- *Inflow boundary.*
  At an inflow boundary we have to specify the velocity, the temperature and all substresses. We assume that these quantities are fully developed. For the calculation we have a simple 1D program. We decouple the temperature equation and the equations of motion. This results in an algebraic equation for the shear rate and an ordinary differential equation for the stresses. The algebraic equation for the shear rate is solved with a simple Picard or secant method. To obtain a convergent scheme we had to add an iteration diffusivity in the

integration of the temperature equation. This procedure is analogous to the finite element temperature equation.

– *Outflow boundary.*
In principle it is possible to impose fully developed boundary conditions at the outflow, as we do for the isothermal calculations. For nonisothermal flows with high Péclet numbers, however, this would require very long exit lengths. This would require long computation times and a large memory capacity of your computer. To avoid this, we impose for the outflow natural boundary conditions that are based on the fully developed flow. The procedure is as follows. For the temperature we suppose a zero heat flux in the normal direction. For the momentum equations we prescribe the normal stress and a zero tangential velocity. The only problem is to find a good approximation of the normal stress at the outflow. We have done that by using the temperature resulting from the natural temperature boundary conditions for calculation of the viscosities and relaxation times. With these calculated viscosities and relaxation times we calculate a fully developed pressure and a fully developed extra stresses, which form the normal stress at the outflow.

4. Problem Description

By Hulsen & van der Zanden (1991) an eight-mode Giesekus model has been used to calculate the steady, isothermal flow of a low density polyethylene (LDPE) melt through a 4 to 1 contraction. For the nonisothermal calculations we have also used this model described by Bird et al. (1987). The viscoelastic material parameters for this model can be found in table I. The thermal properties in table II are also from Bird et al. (1987). So far we know there are no measurements of the anisotropical heat conduction parameters of LDPE. For our calculations we therefore assumed some parameters, which are given in table III. This means that 80% of the heat conduction takes place through the polymer chains. This value is not unusual for rubbers, see van den Brule (1989). In figure 3 and 4 we have plotted the shear viscosity and the elongational viscosity for this model for the temperature range we use in our calculations in section 5.

The temperature boundary conditions we have used for our axisymmetrical examples in section 5 have been plotted in figures 5 and 6. In the first example the wall near the vortex has been heated. In the second example the wall has been cooled from the contraction to the outflow. On the fixed wall we have assumed that the no-slip boundary condition holds for the equations of motion. For the inflow and outflow we have prescribed fully developed profiles as described in subsection 3.4.

For our calculations we varied two dimensionless numbers, the Deborah number and the Péclet number. Because of the problems with the calculation of the dissipation for the 3D Giesekus model we didn't look more closely at the influence of the dissipation. In our examples the temperature rise due to dissipation is small, less than $0.5K$. Both the dimensionless numbers are calculated at the outflow. The Deborah number, which denotes the ratio of the characteristic time scale of the fluid

TABLE I
Viscoelastic properties of LDPE, from Bird et al. (1987)

k	η_k(Pa · s)	λ_k(s)	α_k
1	$1.00 \cdot 10^3$	10^3	0.03
2	$1.80 \cdot 10^4$	10^2	0.05
3	$1.89 \cdot 10^4$	10^1	0.2
4	$9.80 \cdot 10^3$e	10^0	0.5
5	$2.67 \cdot 10^3$	10^{-1}	0.4
6	$5.86 \cdot 10^2$	10^{-2}	0.3
7	$9.48 \cdot 10^1$	10^{-3}	0.2
8	$1.29 \cdot 10^1$	10^{-4}	0.1

TABLE II
Thermal properties of LDPE, from Bird et al. (1987)

ρ	$7.82 \cdot 10^2$kg/m^3
c_p	$2.57 \cdot 10^3$J/kgK
κ	$2.41 \cdot 10^{-1}$W/mK
T_{ref}	423K
c_1	$4.50 \cdot 10^3$K

TABLE III
Heat conduction constants in (W/mK) for all modes k

κ_0	$4.82 \cdot 10^{-2}$
$\kappa_{1,k}$	$2.41 \cdot 10^{-2}$
$\kappa_{2,k}$	0

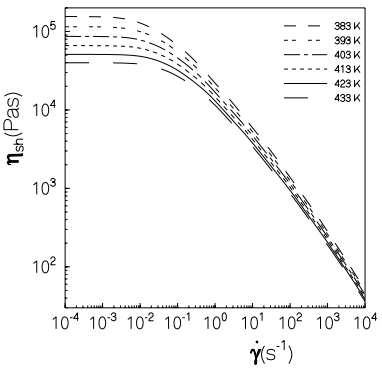

Fig. 3. Shear viscosity for the LDPE melt versus shear rate at different temperatures.

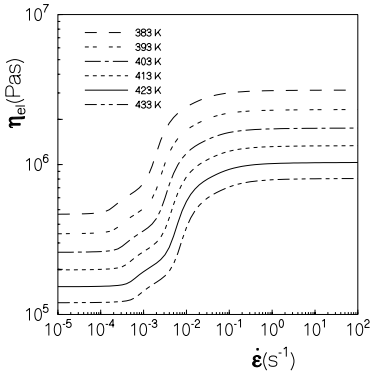

Fig. 4. Elongational viscosity for the LDPE melt versus shear rate at different temperatures.

and a characteristic time scale of the flow, is defined by

$$De = \frac{\lambda_{0,\text{ref}} \langle v \rangle}{D_d},$$

with $\langle v \rangle$ the average velocity and D_d the diameter at the outflow. The mean relaxation time at reference temperature $\lambda_{0,\text{ref}}$ is defined as

$$\lambda_{0,\text{ref}} = \sum_{k=1}^{K} \frac{\lambda_{k,\text{ref}} \eta_{k,\text{ref}}}{\eta_{0,\text{ref}}},$$

with $\eta_{0,\text{ref}} = \eta_{s,\text{ref}} + \sum_{k=1}^{K} \eta_{k,\text{ref}}$ the zero-shear-rate viscosity at reference temper-

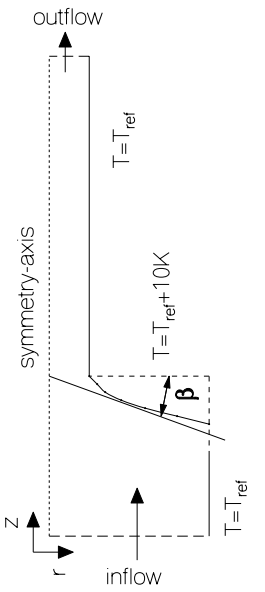

Fig. 5. Boundary conditions for problem 1 and definition of the opening angle β. The wall near the vortex (dashed line) has been heated. The other part of the wall has been kept at reference temperature.

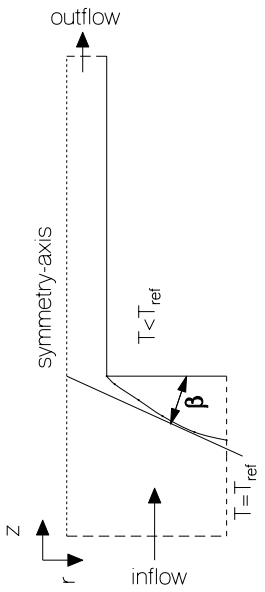

Fig. 6. Boundary conditions for problem 2. The wall at the inflow (dashed line) has been kept at reference temperature. The other part of the wall (straight line) has been cooled.

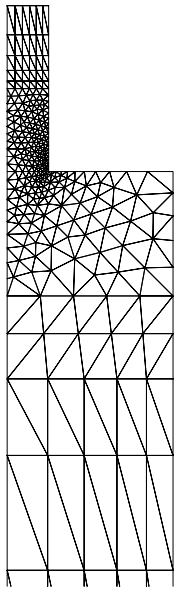

Fig. 7. A part of the finite element mesh near the sharp corner.

ature. The Péclet number, denoting the ratio of the convective transport and the transport by conduction, is based on the equilibrium thermal conductivity coefficient:

$$Pe = \frac{\rho c_p \langle v \rangle D_d}{2\kappa_{\mathrm{eq}}}.$$

We have examined three characteristic quantities for the flow through a contraction. Firstly the opening angle β, defined in figure 5. The second quantity is the vortex intensity, the ratio of the amount of fluid flowing in the vortex and in the main flow:

$$I_\psi = \frac{\psi_{\mathrm{sep}} - \psi_{\mathrm{cen}}}{\psi_{\mathrm{axis}} - \psi_{\mathrm{sep}}},$$

where ψ is the stream function value at the separating streamline ψ_{sep}, the centre of the vortex ψ_{cen} and the symmetry axis ψ_{axis}. Finally we examine an entrance correction, defined by

$$n_c^{\mathrm{iso}} = \frac{-\sigma_n^{\mathrm{en}} + \sigma_n^{\mathrm{ex}} - \left(\Delta p_{\mathrm{en}}^{\mathrm{dev}} + \Delta p_{\mathrm{ex}}^{\mathrm{dev}}\right)^{\mathrm{iso}}}{2\tau_w^{\mathrm{iso}}}.$$

σ_n^{en} and σ_n^{ex} are the total normal stresses at the wall of the entry and exit. $\Delta p_{\mathrm{en}}^{\mathrm{dev}}$ and $\Delta p_{\mathrm{ex}}^{\mathrm{dev}}$ are the pressure differences in the entrance and exit region that would

exist if the isothermal flow at reference temperature was fully developed. The quantity is normalized with the wall shear stress from the isothermal flow at reference temperature. For isothermal flows this quantity gives the extra pressure loss due to the contraction. For nonisothermal flows there is also an effect due to the cooling or heating of the fluid.

For our computations we have used a HP9000-720 computer with a Linpack speed of 14 Mflops and a HP9000-735 computer with a Linpack speed of 40 Mflops. To obtain a converged solution we used an iteration viscosity of $\eta_{\rm it} = 2\eta_0$, $\eta_{\rm co} = \eta_0$ and for the nonisothermal problems $\kappa_{\rm it} = 5\kappa_{\rm eq}$. For the isothermal calculation with a Deborah number of 100 the largest number of iterations were needed, 189 iterations which took 6 seconds per iteration on the HP9000-735. For the nonisothermal problems, with $De = 10$, we needed 40 - 60 iterations, which took 15-20 seconds per iteration on the HP9000-735. The mesh we have used consists of 1452 nodal points. To give an idea of the mesh we have plotted the part near the sharp corner in figure 7. The mesh is rather coarse near the inflow and outflow boundary. It has been refined towards the sharp corner, where large gradients are present. The inflow length is $L_u = 20D_d$ and the outflow length $L_d = 60D_d$.

5. Results

In this section we will examine the influence of the Deborah number, the Péclet number and the cooling temperature on the flow. Figure 8 shows the influence of the Deborah number for isothermal flows. The opening angle β becomes larger when the Deborah number increases. The idea is that the growth of the vortex is a mechanism to fulfil the balance of momentum in the z-direction:

$$\frac{1}{r}\frac{\partial r\tau_{rz}}{\partial r} + \frac{\partial \tau_{zz}}{\partial z} \simeq 0, \tag{34}$$

where we have neglected the pressure gradient. The build-up of the dominant term in this equation, τ_{zz}, before the contraction can be more gradually with a larger vortex. For low Deborah numbers the vortex intensity increases with increasing De. For high Deborah numbers the vortex intensity slowly decreases with increasing De. Some numerical values can be found in table IV.

For all the nonisothermal examples with boundary conditions defined in figure 5 and 6 the opening angle didn't change significantly. The influence of the temperature changes was too small or too locally. The differences in the vortex intensities, however, are relatively large.

For problem 1 the heating has two opposite effects. On the one hand the vortex intensity is decreased. An increase in the temperature gives rise to a fluid that is less elastic. A temperature rise of $10K$ of the whole fluid with $De = 10$ corresponds to an isothermal flow with $De = 7.8$. In this region the vortex intensity increases with increasing elasticity, see table IV. On the other hand the vortex intensity will be increased due to the temperature differences in the flow. Due to the higher temperatures in the vortex region, the viscosity is locally smaller than in the main flow. This results in larger velocities in the vortex and consequently larger vortex intensities. In table V we see that for the isotropic heat conduction the first effect is dominant for the lowest Péclet number and the second effect is dominant for the

TABLE IV
Vortex intensity and opening angle for different Deborah numbers

De	$I_\psi(\%)$	β(deg)
1	1.8	25
7.8	10.8	47
10	11.3	47
100	10.5	58

TABLE V
Vortex intensity for different Péclet numbers for problem 1. The first column is without anisotropy, the second with the anisotropy parameters from table III. The Deborah number equals $De = 10$.

Pe	$I_\psi(\%)$	$I_\psi^a(\%)$
10	11.1	12.1
100	12.4	12.4
1000	12.6	12.6

others. The reason for this can be seen in figure 9. For the lowest Pe the temperature difference between the vortex and the main flow is relatively small, in contrary to the other Péclet numbers. In table V and figure 10 the influence of the anisotropy on the vortex intensity and the temperature field can be found. For the smallest Péclet number the influence of the anisotropy is relatively large. The anisotropy of the heat conduction influences the temperature field near the contraction drastically. Due to the large elongational stresses the polymer chains will be oriented in the direction of the flow. This results in an increase of the heat flux in the direction of the flow and a decrease in the direction perpendicular to it. This results in a larger temperature difference between the vortex region and the main flow, and consequently a larger vortex intensity. For $Pe = 100$ and $Pe = 1000$ the flow is too convection dominant to give large differences between the figures 9 and 10. There are only small differences near the sharp corner, where the stresses are relatively large and the velocity is relatively small.

In the second example we will examine the influence of the cooling temperature. Again the influence on the opening angle is relatively small. The influence on the vortex intensity and the entrance correction has been summarized in table VI. For these calculations $De = 10$, $Pe = 1000$ and anisotropy is taken into account. Due to the cooling of the wall the temperature in the vortex and outflow region becomes lower. In the vortex region, however, the cooling is more effective. Firstly because the velocity is smaller and thus the local Péclet number is smaller in the vortex region. Secondly because the stresses in the outflow region are larger, which results in a stronger orientation of the polymer chains. This gives a reduction in the heat conduction in the r-direction. This results in a decreasing vortex intensity for a decreasing wall temperature. Additionally we calculated the entrance corrections for the different cooling temperatures. Due to the low thermal diffusion perpendicular to the flow direction compared to the convective transport parallel to the flow the cold temperature boundary layer develops very slowly along the wall. Consequently the temperature profile is far from fully developed at the outlet and near the symmetry axis there is no decrease of the temperature at all. This can be seen in figure 11, where the temperature isolines have been plotted for 1/6 of the exit length and 3/10

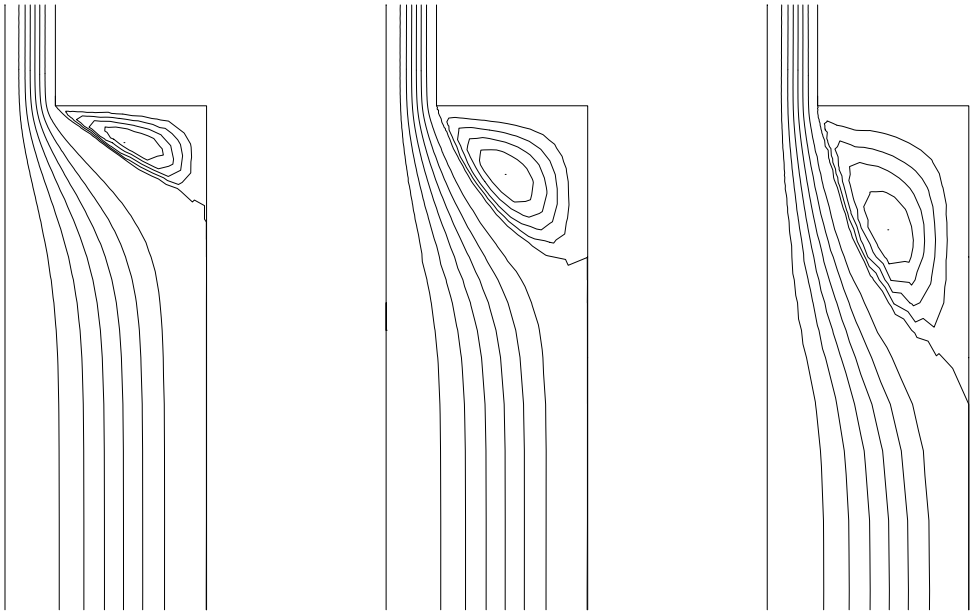

Fig. 8. Streamlines for isothermal flows with increasing Deborah number. $De = 1$, $De = 10$ and $De = 100$.

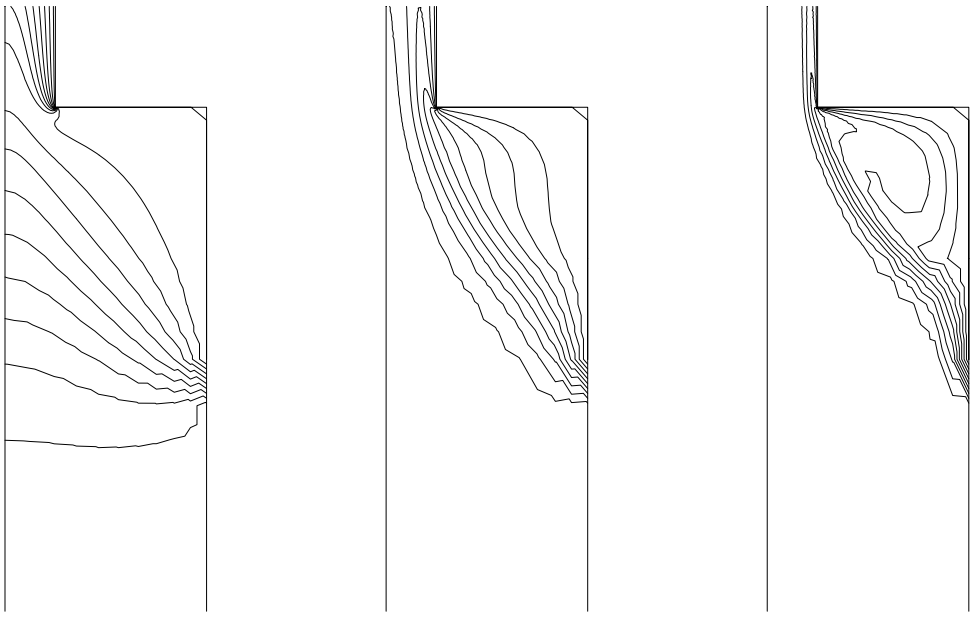

Fig. 9. Temperature isolines for increasing Péclet numbers for problem 1. $Pe = 10$, $Pe = 100$ and $Pe = 1000$, without anisotropic heat conduction. Each isoline differs about $0.9K$ from the next one.

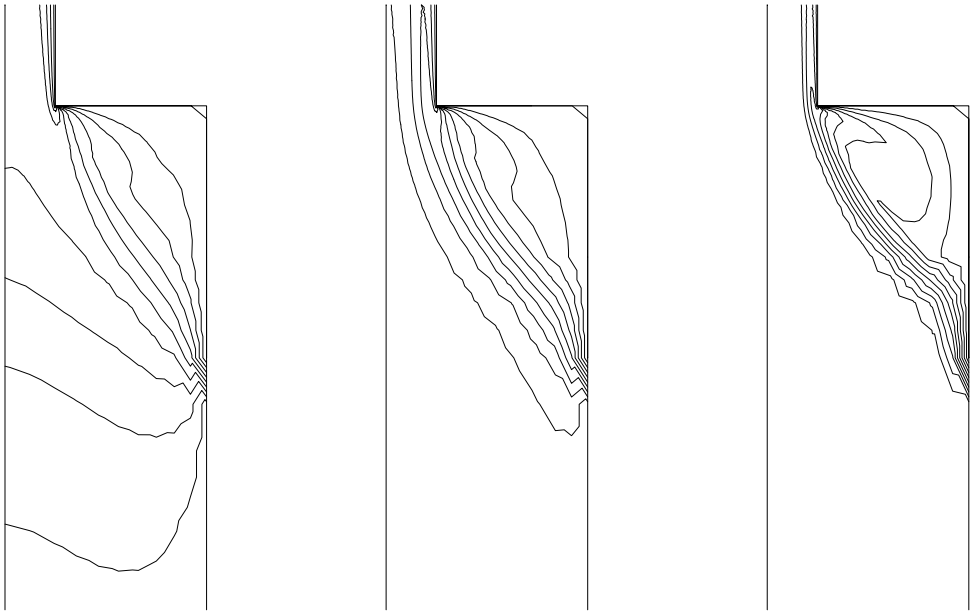

Fig. 10. Temperature isolines for increasing Péclet numbers for problem 1. $Pe = 10$, $Pe = 100$ and $Pe = 1000$, with anisotropic heat conduction. Each isoline differs about $0.9K$ from the next one.

of the entry length. The isoline nearest to the axis of symmetry is only $1K$ below the reference temperature. Figure 11 also shows that a relatively large part of the cold layer in the exit is due to the convection from the entry region. In this region the local Péclet number is smaller, so the cold front can penetrate more easily in the main flow there. Although the cold temperature layer is relatively small in radial direction the influence on the magnitude of the entrance correction is large compared to the isothermal flow. For the lowest wall temperature the entrance correction is more than 10 times larger than for the isothermal flow. Note that the magnitude of n_c^{iso} depends strongly on the exit length, the longer the exit length the larger n_c^{iso}. Of course it would be better to have a quantity that does not depend on the exit length. This is however very difficult, if not impossible, because the cold layer is determined by both convection from the vortex region and diffusion from the cold wall in the exit.

6. Concluding remarks

We have extended the numerical implementation of Hulsen & van der Zanden (1991) for steady and isothermal flow of viscoelastic fluids with some nonisothermal effects. The viscosities and relaxation times have been made temperature dependent by means of a shift factor. In the energy equation two effects that are special for viscoelastic fluids have been taken into account. The first is the anisotropy of the heat conduction due to molecular orientation of the polymer chains. The second is storage

TABLE VI
Shift factor at the cooled wall, vortex intensity and entrance correction for different cooling temperatures at the wall.

T_{wall}(K)	a_T^{wall}	I_ψ(%)	n_c^{iso}
423	1.00	11.3	1.5
413	1.29	10.1	5.6
403	1.70	8.8	10.3
393	2.25	7.4	15.4
383	3.04	6.1	20.9

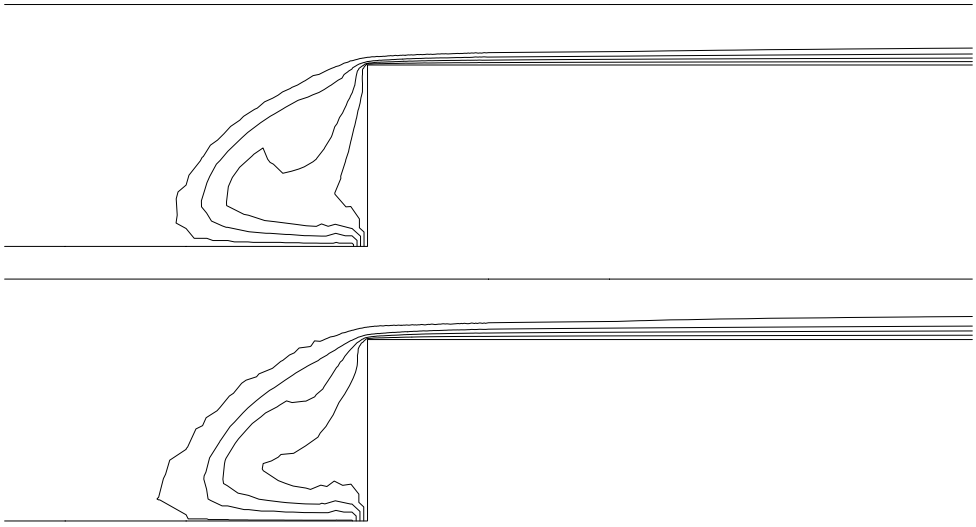

Fig. 11. Temperature isolines for different wall cooling temperatures (30% of the entry length and 16% of the exit length). For $T_{\text{wall}} = 413K$ the isolines are between $T = 413K$ and $T = 422K$. For $T_{\text{wall}} = 383K$ the isolines are between $T = 383K$ and $T = 422K$.

of elastic energy, through which the dissipation does not equal the stress work. For the axisymmetrical Giesekus model we used, we have still some problems for the calculation of this quantity near sharp corners. This is caused by the indefiniteness of the internal deformation tensor.

In our examples we examined the influence of the Péclet number, the anisotropical heat conduction and the wall cooling on the flow. The influence on the opening angle and the main flow velocity is small. The vortex intensity and the entrance correction, however, show large differences. The influence of the anisotropical heat conduction is relatively small for high Péclet numbers.

Acknowledgements

We want to acknowledge J.P.P.M. van der Zanden for his advices and help with the extension of the numerical code to nonisothermal flows and G.D.C. Kuiken for his comments on this work.

References

Bird, R.B., Armstrong, R.C. & Hassager, O.: 1987, 'Dynamics of polymeric liquids', Vol. 1 2nd edn., Wiley, New York

Brule, B.H.A.A. van den: 1989, 'A network theory for the thermal conductivity of an amorphous polymeric material', *Rheol. Acta* Vol. no. **28** pp. 257-266

Brule, B.H.A.A. van den: 1990, 'The non-isothermal elastic dumbbell: a model for the thermal conductivity of a polymer solution', *Rheol. Acta* Vol. no. **29** pp. 416-422

Crochet, M.J.: 1989, 'Numerical simulation of viscoelastic flow: a review', *Rubber Chem. Technol.* Vol. no. **62** pp. 426–455

Giesekus, H.: 1982, 'A simple constitutive equation for polymer fluids on the concept of deformation-dependent tensorial mobility', *J. Non-Newtonian Fluid Mech.* Vol. no. **11** pp. 69–109

Hands, D.: 1980, 'The effect of biaxial orientation on the thermal coductivity of vulcanized and unvulcanized rubber', *Rubber Chem. Technol.* Vol. no. **53** pp. 80–87

Hughes, T.J.R. & Brooks, A.: 1982, 'A theoretical framework for Petrov- Galerkin methods with discontinuous weighting functions: application to the streamline-upwind procedure' *Finite elements in fluids* (ed. Gallagher, R.H., Norrir, D.H., Oden, J.T. & Zienkiewicz, O.C.), Vol. no. 4, Wiley, New York, pp. 47–65

Hulsen, M.A.: 1988, 'Some properties and analytical expressions for plane flow of Leonov and Giesekus models', *J. Non-Newtonian Fluid Mech.* Vol. no. **30** pp. 85–92

Hulsen, M.A.: 1990, 'A sufficient condition for a positive definite configuration tensor in differential models', *J. Non-Newtonian Fluid Mech.* Vol. no. **38** pp. 93–100

Hulsen, M.A. & van der Zanden, J.P.P.M.: 1991, 'Numerical simulation of contraction flows using a multi-mode Giesekus model', *J. Non-Newtonian Fluid Mech.* Vol. no. **38** pp. 183–221

Jongschaap, R.J.J.: 1991, 'Towards a unified formulation of microrheological models', *Lecture Notes in Physics* Vol. no. **381**, pp. 215–247

Keunings, R.: 1989, 'Simulation of viscoelastic fluid flow', *Fundamentals of computer modeling for polymer processing* (ed. Tucker, C.L. III), Carl Hanser Verlag, pp. 403–469

Leonov, A.I.: 1987, 'On a class of constitutive equations for viscoelastic liquids', *J. Non-Newtonian Fluid Mech.* Vol. no. **25** pp. 1–59

Mizukami, A. & Hughes, T.J.R.: 1985, 'A Petrov-Galerkin finite element method for convection dominated flows: an accurate upwinding technique for satisfying the maximum principle', *Comp. Meth. Appl. Mech. Eng.* Vol. no. **50** pp. 181–193

Washo, B.D. & Hansen, D.: 1969, 'Heat conduction in linear amorphous high polymers: orientation anisotropy', *J. Appl. Phys.* Vol. no. **7** pp. 2423–2427